Aeolian Research 59 (2022) 100840

Contents lists available at ScienceDirect

Aeolian Research

journal homepage: www.elsevier.com/locate/aeolia

Cellular automaton modelling of the effects of buildings on aeolian bedform dynamics

Daan W. Poppema [a,b,*], Andreas C.W. Baas [c], Suzanne J.M.H. Hulscher [a], Kathelijne M. Wijnberg [a]

[a] Water Engineering and Management, University of Twente, 7500 AE Enschede, The Netherlands
[b] Department of Hydraulic Engineering, Delft University of Technology, 2600 GA Delft, The Netherlands
[c] Department of Geography, King's College London, 30 Aldwych, WC2B 4BG London, United Kingdom

ARTICLE INFO

Keywords:
Anthropogenic effects
Sediment dynamics
Obstacles to wind flow
Beach buildings

ABSTRACT

Buildings affect aeolian sediment transport and bedform development in sandy environments. Cellular automaton (CA) models have, however, only been used to simulate natural bedform dynamics. This study extends a well-known aeolian CA model to include sediment dynamics around buildings, and uses this model to explore the interaction of building-induced deposition and erosion with natural bedform dynamics. New CA rules are introduced to represent acceleration, deceleration and sideward transport of sediment around obstacles. The simulated deposition and erosion patterns show good agreement with field experiments. The model reproduces the shape and location of the morphological pattern around a single building, and effects of building spacing on this pattern for building groups. Model results further demonstrate that building-induced effects interact with local bedform dynamics and can alter the shape, growth and migration of sand dunes.

Introduction

Buildings constructed in environments with active aeolian sediment transport, such as deserts or beaches, affect local morphodynamics. As unerodable, bluff objects, buildings change the wind field in their surroundings (Hunt, 1971; Nordstrom and McCluskey, 1985), create patterns of erosion and deposition (Luo et al., 2012; Poppema et al., 2021), and act as an obstacle to sediment transport (Jackson and Nordstrom, 2011). Cities, bridges and other infrastructure in deserts and dune fields have also been shown to alter wind speed, wind direction, sediment transport capacity, and vegetation cover in their surroundings, and can cut off dune fields from their sediment source (Malvarez et al., 2013; Hernández-Calvento et al., 2014; Smith et al., 2017b; Bruno et al., 2018; Wang et al., 2020).

Deposition and erosion around buildings can have considerable consequences for surrounding infrastructure. Building entrances, walkways, and roads may be blocked by sand deposition (Jackson and Nordstrom, 2011) and in coastal settings there may be repercussions for flood safety, for instance with local scour around buildings creating a weak spot in the dunes (Nordstrom and McCluskey, 1984, 1985). In addition, locally increased deposition around buildings may intercept sediment transport into coastal dunes (Hoonhout and Van Thiel de Vries, 2013; Reinders et al., 2014), reducing dune growth and coastal safety in a larger area. Dune migration can also cause extensive damage to buildings in deserts (Lorenz et al., 2013; Abbasi et al., 2019) or coastal environments (Sherman and Nordstrom, 1994).

Existing studies on the morphological effects of buildings have focused on the local effects in a uniform flat environment, using scaled field experiments at the beach (Poppema et al., 2021; Poppema et al., 2022c) or in wind tunnel experiments (Iversen et al., 1990; Luo et al., 2012; McKenna Neuman et al., 2013; Luo et al., 2014; McKenna Neuman and Bédard, 2015; Luo et al., 2016). However, deserts and beach-dune systems are dynamic environments that exhibit strong bedform dynamics. Building-induced deposition and erosion features are not formed statically in a flat landscape, but they interact with self-organizing bedform dynamics and change under influence of fluctuating wind directions and conditions.

Aeolian bedform dynamics have been studied extensively using Cellular automaton (CA) models (Werner, 1995; Baas, 2002; Nield and Baas, 2008; Eastwood et al., 2011; Barchyn and Hugenholtz, 2012; Zhang et al., 2012). These models describe aeolian sand transport using relatively simple rules, which through self-organization lead to

* Corresponding author at: Department of Hydraulic Engineering, Delft University of Technology, 2600 GA Delft, The Netherlands.
E-mail address: d.w.poppema@tudelft.nl (D.W. Poppema).

https://doi.org/10.1016/j.aeolia.2022.100840
Received 11 February 2022; Received in revised form 14 October 2022; Accepted 4 November 2022
Available online 18 November 2022

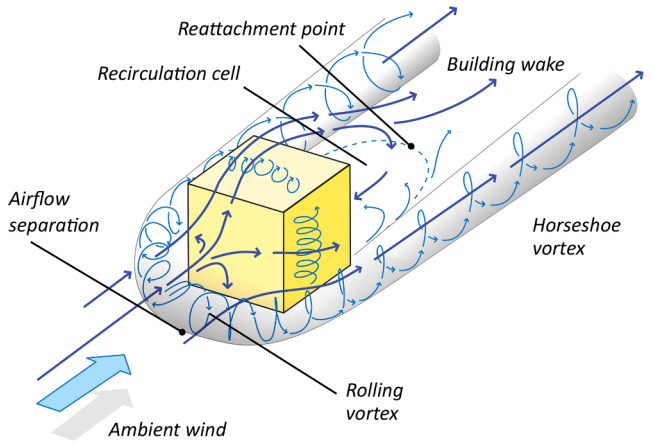

Fig. 1. Conceptual airflow patterns around a building oriented perpendicular to the wind adapted from (Oke et al., 2017).

remarkably complex bedform dynamics (Baas, 2002; Fonstad, 2013). The seminal Werner Algorithm (Werner, 1995) models sand transport as sand slabs moving over a grid with spatially varying probabilities of slab erosion and deposition. This algorithm successfully models the formation of barchan, linear and star dunes. The DECAL model (Discrete ECogeomorphic Aeolian Landscape model) adds vegetation dynamics, allowing for the formation of parabolic dunes (Baas, 2002, 2007; Nield and Baas, 2008). The Dubeveg (Dune Beach Vegetation) model further adds hydrodynamic beach dynamics and implements groundwater as limiting factors for aeolian erosion, to model coastal beach-dune systems (De Groot et al., 2011; Keijsers et al., 2016). The feedbacks and interactions between all these processes allow for a wide range of applications, such as the effect of vegetation characteristics on dune dynamics (Nield and Baas, 2008; Yan and Baas, 2017), of sea level rise on dune evolution (Keijsers et al., 2016) and of groundwater on coastal dune development (Galiforni Silva et al., 2018).

This model is used as basis for this study, because its performance in capturing the spatial interactions between processes makes it suitable to study feedbacks between building-induced bed patterns and natural bedforms, and the resulting spatial distribution of sediment. Moreover, compared to process-based models such as the Coastal Dune Model (Duran and Moore, 2013), Aeolis (Hoonhout and De Vries, 2016) or Duna (Roelvink and Costas, 2019), the model has advantages in the model flexibility for adding building effects, the range of coastal processes that can be included, and the run-time for yearly to decadal simulations.

This study aims to: 1) extend these morphodynamic CA models with effects of buildings, and 2) use this to explore how building-induced morphological patterns interact with self-organized aeolian bedform dynamics. We develop new CA rules for the effects of buildings on local sediment transport. To test the performance of these rules, CA results of scenarios with buildings are compared to results of field experiments with individual scale models of various sizes (Poppema et al., 2021; data available as Poppema et al., 2022b) and scale model groups of various building spacings (Poppema et al., 2022c; data available as Poppema et al., 2022a). Longer-term model scenarios (up to decadal time scale) are used to explore interactions between self-organized bedform dynamics and building-induced deposition and erosion.

Background: Deposition and erosion around buildings

The morphological effect of a building on its surroundings starts with a building obstructing airflow and aeolian sediment transport. Upwind of a building, a portion of the airflow hitting the building is deflected downwards, creating a rolling vortex in front of the building. This rolling vortex is then wrapped around the building, forming a horseshoe vortex structure (Fig. 1). In sandy environments, the flow reversal in front of a building placed on the ground (i.e. not on stilts) creates deposition a small distance upwind of the building, similar to echo dunes in front of natural cliffs (Tsoar, 1983; Tsoar and Blumberg, 1991; Qian et al., 2011). In experiments with cliffs over the entire wind tunnel width, Tsoar (1983) found the distance from dune crest to cliff to be approximately 0.6 times the cliff height. However, field experiments we conducted with cuboid scale models of buildings on the beach (Poppema et al., 2021) showed that the deposition size and location around buildings are also determined by building width, because wider buildings intercept more sand and create a larger vortex in front of the building.

Sand that is not deposited in front of the building is mainly blown around rather than over the building: most sand transport occurs close to the bed and follows the horseshoe vortex structure. This often creates downwind deposition near the horseshoe vortex tails (Poppema et al., 2021). At the building sides, wind speed and sediment transport are increased due to sand and wind diverted around the building. As wind speed slowly reverts to the undisturbed conditions, the sediment transport capacity decreases, explaining the downwind deposition. Apart from wind speed, the complex 3D flow field also plays a role here, with horizontal convergence promoting deposition in the horseshoe vortex tails (Pourteimouri et al., 2022). Directly adjacent to a building, the accelerated airflow can create scour. However, lateral deposition is also possible here, similar to the downwind deposition tails. Finally, in the lee behind the building, erosion can occur, due to sediment being diverted around the buildings leading to a lower sediment influx. However, the flow deceleration in this area also decreases the sediment transport capacity, so if sediment enters the area directly behind the building, this can create deposition (Luo et al., 2012; Poppema et al., 2019). This deposition in the lee of an object is alternatively referred to as a sand shadow (Bagnold, 1941; Luo et al., 2012); shadow dune or lee dune (Hesp, 1981; Cooke et al., 1993; Pye and Tsoar, 2008); or leeward drift (Beyers and Waechter, 2008).

When multiple buildings are placed close together, this changes the airflow pattern and thereby the morphological effect. For a row of adjacent buildings, the effect depends on the building spacing. At smaller building spacings, airflow and sediment transport through the gaps between buildings is limited, as wind and sand are predominantly diverted around the building group (Thiis and Jaedicke, 2000; Yen and Liu, 2011; Luo et al., 2014). As shown by the scale experiments at the beach (Poppema et al., 2022c), this creates downwind deposition tails at the outside of the building group that are larger than the deposition tails behind the gaps. If building spacing increases, wind and sand increasingly flow through the gaps instead of around the building group. As a result, deposition outside of the building group decreases, while it increases behind the gaps. For large building spacing, airflow and sediment transport around each building are barely affected by the neighbouring building, and the morphological pattern is almost a superposition of the deposition and erosion expected around individual buildings. For buildings with an approximately square wind-facing surface, this occurs for a building spacing of more than approximately 2 buildings widths. Locally, erosion can occur in the gaps between buildings and directly behind gaps, due to the high velocity of wind funnelled through the gaps.

Methodology

Model description

The model used in this study is an extension of Werner (1995), where the domain consists of a cellular grid covered with stacks of slabs of a fixed thickness to represent topography. Sediment transport occurs stochastically by the movement of slabs in orthogonal directions, with periodic boundary conditions at the grid edges. Sediment transport starts by random selection of cells to be eroded, where the top slab of

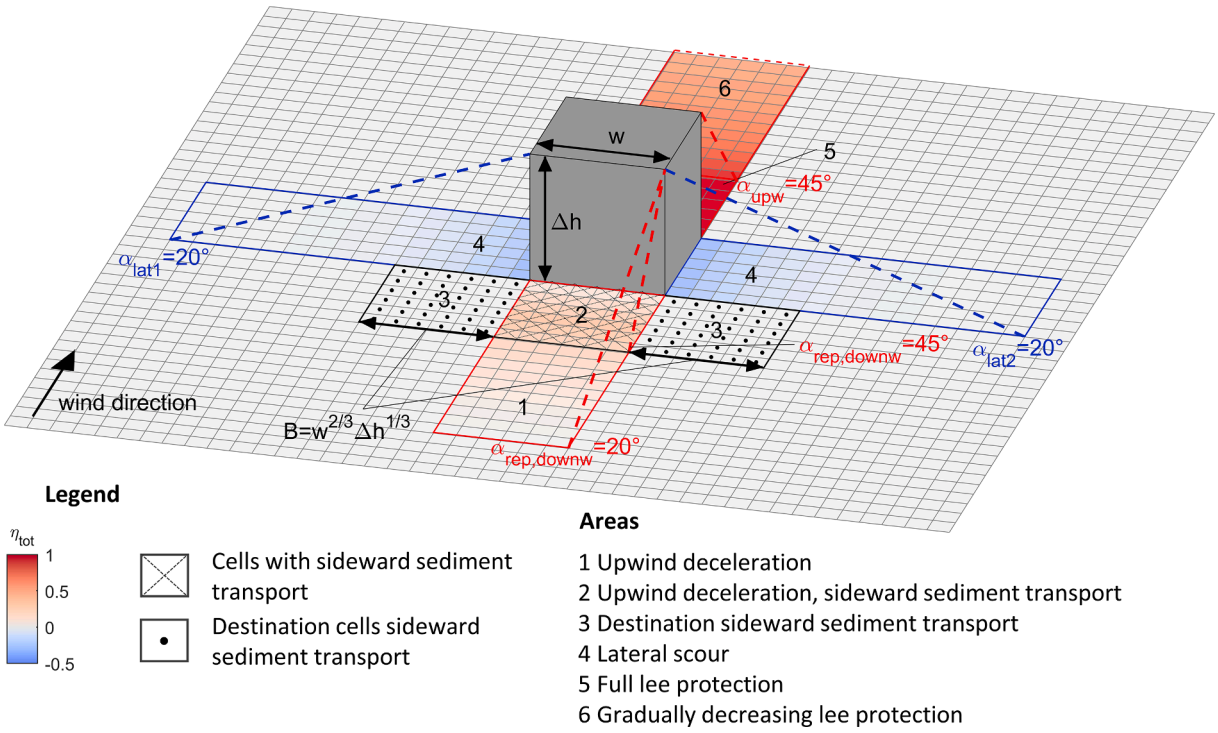

Fig. 2. A sketch of the CA model, indicating in which areas a building affects the cumulative deposition effectiveness η_{tot}, and hence p_e and p_d.

every cell has a probability p_e to be eroded. Eroded slabs are then moved one cell downwind, where they have a probability p_d to be deposited. If not, they are moved to the next cell and the process is repeated. When all eroded slabs are deposited, the angle of repose is enforced by avalanching: slabs are shifted in the direction of the steepest slope whenever the slope between cells is larger than 30°.

Shadow zones behind dunes are essential for dune formation in the model (Nield and Baas, 2008). These shadow zones represent the sheltered area behind relief where flow deceleration or recirculation occurs, leading to accretion and dune growth behind a dune and thereby to dune migration. Originally, Werner (1995) implemented this as zones with a p_d value of 1 for cells behind relief that are enclosed by a line of 15° to horizontal. In nearly all following work (Momiji et al., 2000; Baas, 2002; Nield and Baas, 2008; Eastwood et al., 2011; Keijsers et al., 2016; Galiforni Silva et al., 2018), the erosion probability was additionally set to zero, for shadow zones with immediate deposition and no erosion.

The model implementation of this study does not contain vegetation. This makes for a fairer comparison with the field experiments, which were performed on a sandy beach without vegetation. In this sense the model is more similar to the original Werner bare-sand model (Werner, 1995) than to the later DECAL (Baas, 2002) or Dubeveg (Keijsers et al., 2016) models.

Time evolution is represented through repeated iterations of erosion, deposition and avalanching. The time step and spatial scale follow from the combined parameter settings for the cell size, slab height, erosion and deposition probability and number of aeolian iterations per year, together setting the potential aeolian sediment transport rate (Nield and Baas, 2008; Keijsers et al., 2016).

Model extension: Buildings

Buildings differ in two key aspects from natural bedforms and dunes: they are static, in the sense that they have a fixed location and configuration, and they have a bluff shape. The fixed state of buildings is implemented in the model by setting bed elevation to the building height and turning off erosion, deposition and avalanching in grid cells with buildings ($p_e = 0$; $p_d = 0$; angle of repose of 90°). Deposition on top of buildings is theoretically possible, but is disregarded in the model, because sediment transport occurs predominantly close to the bed instead of at roof level (Dong et al., 2003; Rotnicka, 2013), and deposition is further impeded by accelerated airflow over buildings and, if present, gabled roofs. However, the bluff building shape requires larger changes to the model. It creates airflow separation, leading to sideward transport of sediment diverted around buildings and to bed level change upwind and next to buildings, in contrast with streamlined dunes whose morphological effects are mainly downwind.

Therefore, new rules are needed to describe sideward transport for sediment diverted around buildings (Fig. 2, area 2 and 3). In addition, rules are needed for the altered pickup and deposition of slabs in three regions around a building. For the deposition upwind of an obstacle (Fig. 2, area 1 and 2) and the scour next to obstacles (area 4), new rules are added. For the downwind effect of an obstacle, the shadow zone rules are adapted (area 5 and 6). In these three regions, p_e and p_d are altered through three spatially varying modifiers: the upwind deposition effectiveness, lateral scour effectiveness and downwind lee protection effectiveness (η_{upw}, η_{lat} and η_{downw}). η_{upw} and η_{downw} range between 0 and 1 (0 % and 100 %), while η_{lat} ranges between 0 and −1 (0 % and −100 %). Positive values increase deposition while decreasing erosion, and vice versa.

These three effectiveness values are summed to derive the cumulative effectiveness (η_{tot}, with values constrained to the range −1 to + 1). η_{tot} modifies the local probabilities of erosion and deposition linearly from their base values. From $\eta_{tot} = 0$ to $\eta_{tot} = 1$, p_d increases linearly from its base value to 1 (immediate deposition) and p_e decreases from its base value to 0 (no erosion). This is identical to the rules for the combined vegetation effectiveness of multiple vegetation species in DECAL and Dubeveg (Nield and Baas, 2008; Keijsers et al., 2016). From $\eta_{tot} = 0$ to $\eta_{tot} = -1$, the behaviour is reversed: p_d decreases linearly from its base value to 0 and p_e increases from its base value to 1.

Horizon angles

Larger buildings affect airflow and morphology in a larger area. We therefore introduce the *horizon angle* to express cell proximity to buildings, relative to the building size. The horizon angle is the slope at

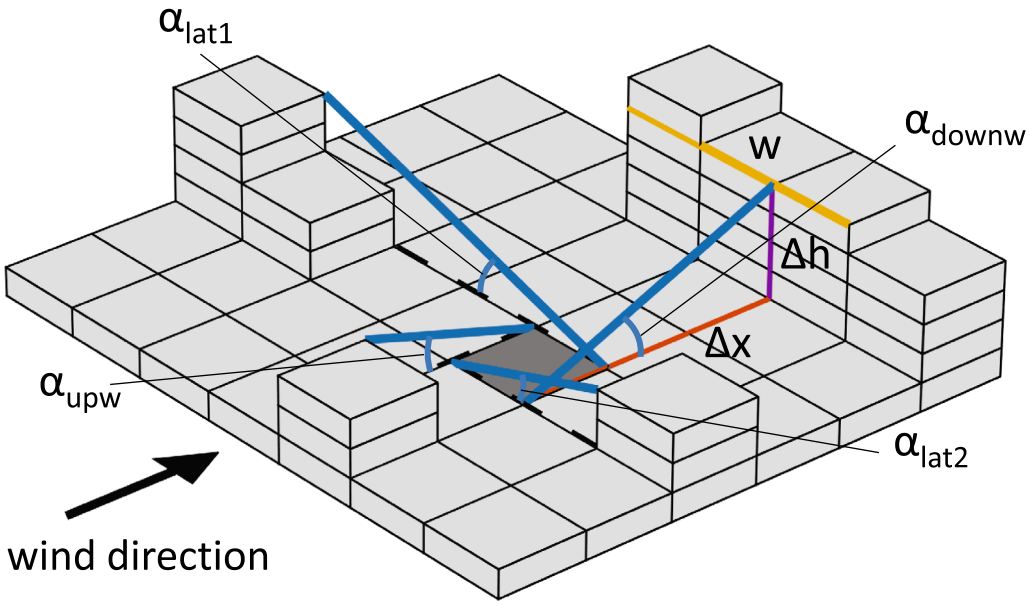

Fig. 3. The horizon angles of a cell, determined in four directions, indicate the slope of the steepest line that still intersects with another cell. The representative downwind horizon angle ($\alpha_{rep,\ downw}$) of a cell is calculated using obstacle width w, combined with the height difference Δh and horizontal distance Δx with the cell intersected by the downwind horizon line (see also the appendix).

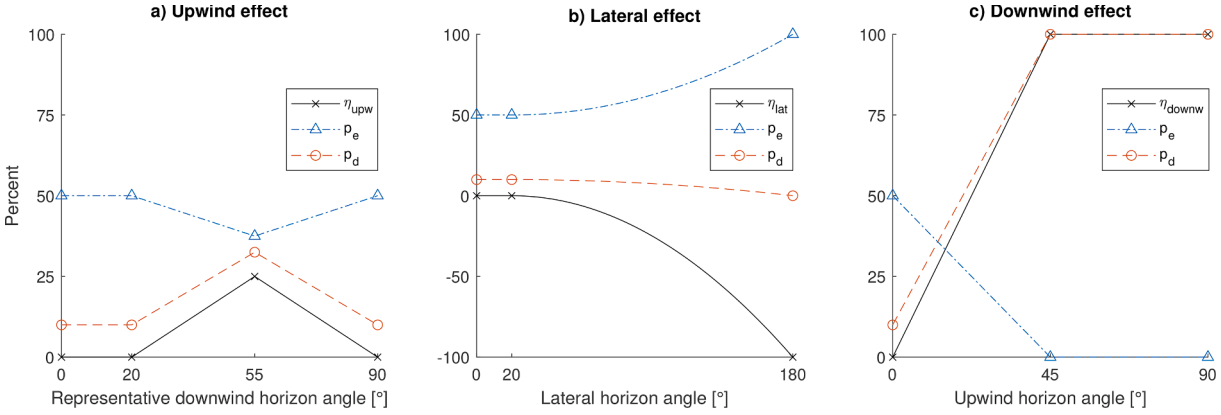

Fig. 4. The horizon angles determine the (a) upwind deposition effectiveness (η_{upw}), (b) lateral scour effectiveness (η_{lat}) and (c) lee protection effectiveness (η_{downw}) and thereby p_e and p_d. and thereby p_e and p_d. The lines for p_e and p_d are based on base values of $p_e = 0.5$ and $p_d = 0.1$.

which an imaginary line, starting from the current level of a cell, intersects exactly with the horizon, measured in the four cardinal directions (Fig. 3). In other words, it is the steepest slope at which the line still intersects with another cell. This other cell can either be a sandy cell (dune) or a building, making the horizon angle a general measure for the entire model domain: there is no distinction between sandy cells and building cells, only the elevation of a cell matters. If a cell is higher than all following cells in a direction, the horizon angle of that direction is set to zero.

The horizon angle only takes into account the height of an obstacle (i.e. dune or building). However, field experiments show that obstacle width also matters: horizontal deposition size scales linearly with building factor B, with $B = w^{2/3} \cdot h^{1/3}$, building width w measured perpendicular to the wind and building height h (Poppema et al., 2021). Therefore, we additionally define a *representative downwind horizon angle* ($\alpha_{rep,\ downw}$), calculated using B instead of the height difference between cells. For the CA implementation, the downwind cell causing the horizon angle is determined first. Next, obstacle width is determined from the number of consecutive neighbouring cells perpendicular to the wind direction with at least the same elevation. For further details, see the appendix on CA model rules.

The erosion and deposition probability around buildings

To model deposition upwind of a building, the representative downwind horizon angle at upwind cells affects the local erosion and deposition probabilities through the *upwind deposition effectiveness* (η_{upw}) defined by the curve shown in Fig. 4a. (Note: *upwind* deposition is linked to the *downwind* horizon angle: if you are located upwind of a building, you see the building by looking in the downwind direction). Next to a building, the strong airflow can scour the bed. Cells located between two obstacles can be subject to more scour than next to a single building, so in the CA model the lateral scour effectiveness η_{lat} depends on the sum of the lateral horizon angles in both directions ($\alpha_{lat} = \alpha_{lat,1} + \alpha_{lat,2}$). For $20^\circ < \alpha_{lat} \leq 180^\circ$, p_e and p_d depend quadratically on the horizon angle (Fig. 4b). In the lee behind buildings, the bed is sheltered, causing flow deceleration and recirculation and thereby deposition (Smith et al., 2017a). Previous CA models already included this effect for dunes, implemented as full deposition ($p_d = 1$) and no erosion ($p_e = 0$) in shadow zones, so in all cells with an upwind horizon angle of more than 15° (Baas, 2002). To represent buildings, which have a constant location

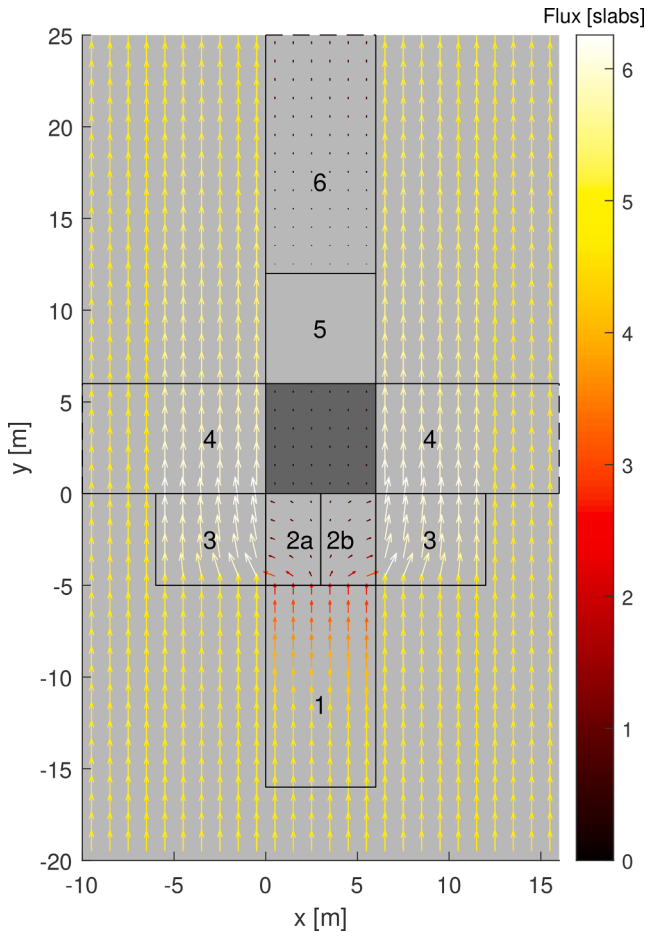

Fig. 5. The average sediment flux pattern around a building of 6 × 6 × 6 m on a flat bed, based on 100 model repetitions of the first aeolian iteration on a flat bed. Arrow colours indicate the sediment flux magnitude, in slabs/cell/iteration. The base flux is 5 slabs/cell/iteration ($p_e/p_d = 0.5/0.1 = 5$). Dark grey cells indicate the building and numbered rectangles the location of the areas described in the text, following the same numbering as Fig. 2.

and large elevation differences with surrounding cells, more nuance is added: a gradual *lee protection effectiveness* replaces the binary shadow zones, so that the effectiveness η_{downw} increases linearly with the horizon angle for $0^\circ < \alpha_{upw} \leq 45^\circ$ (Fig. 4c). For more details on the model rules and the reasoning behind them, see the appendix.

Sideward sediment transport

Buildings do not only change the local deposition and erosion, they also divert sand around them. So the model needs to include some form of sideward sediment transport, i.e. transport perpendicular to the wind direction. Sediment is mainly blown to the side by the rolling vortex directly upwind of a building. This is represented in the model by slabs in transport just upwind of a building having a 50 percent probability of being transported to the side. This applies when $\alpha_{rep,downw}$ is 45° or larger (so within a distance of one building factor B to the building). If moved sideward, slabs are shifted to a cell that is between 1 cell and a distance B at either side of the building. For further details, see the appendix on sideward sediment transport.

Effect of CA rules on sediment flux

The model rules described above produce seemingly realistic sediment transport patterns around a building, with slabs being diverted around and deposition in front of the building (Fig. 5). In area 1 of Fig. 5, upwind deceleration causes the sediment flux to decrease. In area 2, slabs aditionally start being shifted to the side. This causes a sideward flux, stronger at the edge of the area (around x = 0) than at the building's centreline. It also causes a further decrease in the y-component of the flux. Area 3 receives the slabs that were shifted to the side in area 2. This results in an increased sediment flux compared to the undisturbed upwind cells; and in a sideward sediment flux, especially in the grid columns close to the building. In area 4 lateral scour occurs, explaining why the flux is slightly larger in columns directly against the building edge than further away from the building. Although this zone theoretically extends up to a lateral horizon angle of 20°, the scour effectiveness is so weak at the edges of zone 4 that there is no noticeable effect. Area 5 is the zone behind the building where the horizon angle exceeds 45°, so the lee protection effectiveness is 100 %. This means immediate deposition and no erosion, and hence no sediment flux. In area 6, the lee protection effectiveness slowly decreases, allowing for slabs to be picked up from the bed and resulting in an increasing sediment flux.

Model settings

All scenarios start with an initially flat bed and use an erodable sand layer thickness of 1 m, representing the supply limitation that was present in our field experiments due to ground water and, for the full-scale experiment, the development of an armouring layer. A long-term average is used for the erodible sediment thickness – excluding detailed short-term weather effects on surface moisture – based on the large spatial and temporal model scale and long timesteps. All scenarios use a year of 50 aeolian iterations (approximately weekly timesteps), a cell size of 1 × 1 m, base probabilities of $p_e = 0.5$ and $p_d = 0.1$, a slab

Table 1
Description of the model scenarios. Building width is measured in the x-direction, so perpendicular to the wind for unidirectional wind from the south.

Scenario	Duration (year)	Wind direction (%, south + west + east)	Building size (w × l × h, in m)	Group size (# of buildings)	Gap ratio g* (-)
Short term, single building	2	100 + 0 + 0	4,8,12 × 4 × 4; 4,8,12 × 8 × 4; 4,8,12 × 4 × 8	–	–
Short term, multiple buildings	2	100 + 0 + 0	4 × 8 × 4	3	0; 0.33; 0.5; 0.67; 0.75 and 0.8
Short term, wind direction	2	100 + 0 + 0; 67 + 33 + 0; 50 + 50 + 0; 50 + 25 + 25	6 × 6 × 6; 12 × 6 × 6; 6 × 12 × 6	–	–
Long term, single building	15	100 + 0 + 0	10 × 12 × 3	–	–
Long term, wind direction	6	50 + 50 + 0	15 × 15 × 6	–	–
Long term, wind direction 2	15	50 + 50 + 0	25 × 25 × 15	–	–
Long term, building group	12	100 + 0 + 0	10 × 10 × 6	5	0.33
Long term, group + direction	12	67 + 33 + 0	10 × 10 × 6	5	0.33

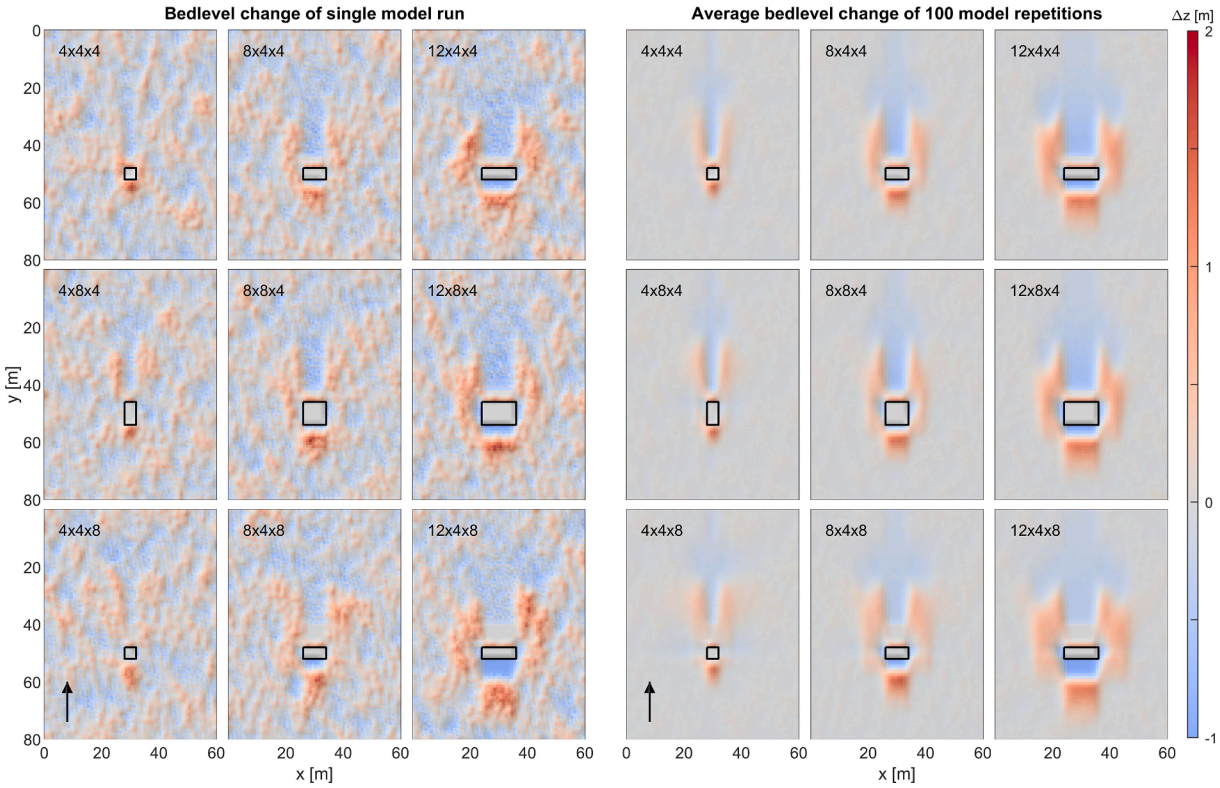

Fig. 6. The topography around single buildings of various sizes after 2 years. Wind is coming from below, building sizes are indicated as w × l × h in metres. The first three columns display the result of a single model repetition, showing both natural bedform dynamics and building-induced effects. The last three columns show the average of 100 model repetitions, to filter out natural bedforms and show consistent building-induced effects.

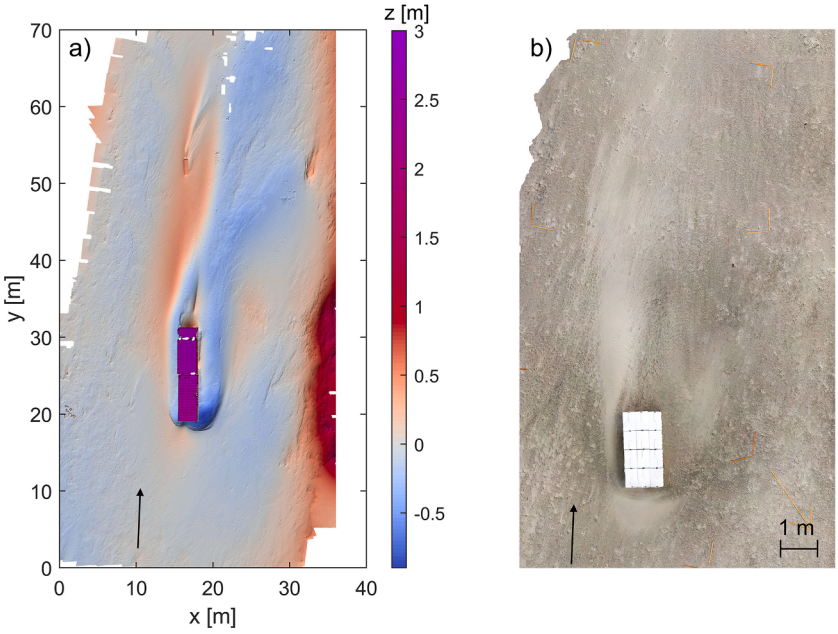

Fig. 7. Examples of results around scale models in the field, with the dominant wind direction from below. Left: A DEM around a scale model of 2.5 × 12 × 2.5 m after 5 weeks in the field. High elevations at the righthand edge of the graph are the dune toe. Deposition is further affected by a small scale model at x,y = 17,52. For details, see Poppema et al. (2021). Right: An orthophoto of the deposition around a scale model of 1 × 2 × 0.35 m, with lighter colours indicating deposition. Result after 1 day.

thickness of 0.1 m and 30° for the angle of repose. These values are based on previous studies of Dutch dune dynamics with Dubeveg (Keijsers et al., 2016; Galiforni Silva et al., 2018; Galiforni Silva et al., 2019) and result in a potential sediment flux of 25 m^3/m/year.

Model scenarios

Both short-term and long-term scenarios are examined with the model. For the short-term scenarios, the model is run for two years (100 aeolian iterations) to focus on the period in which the morphological effects from the building dominate local bedform dynamics. First the modelled morphological development under a unidirectional wind

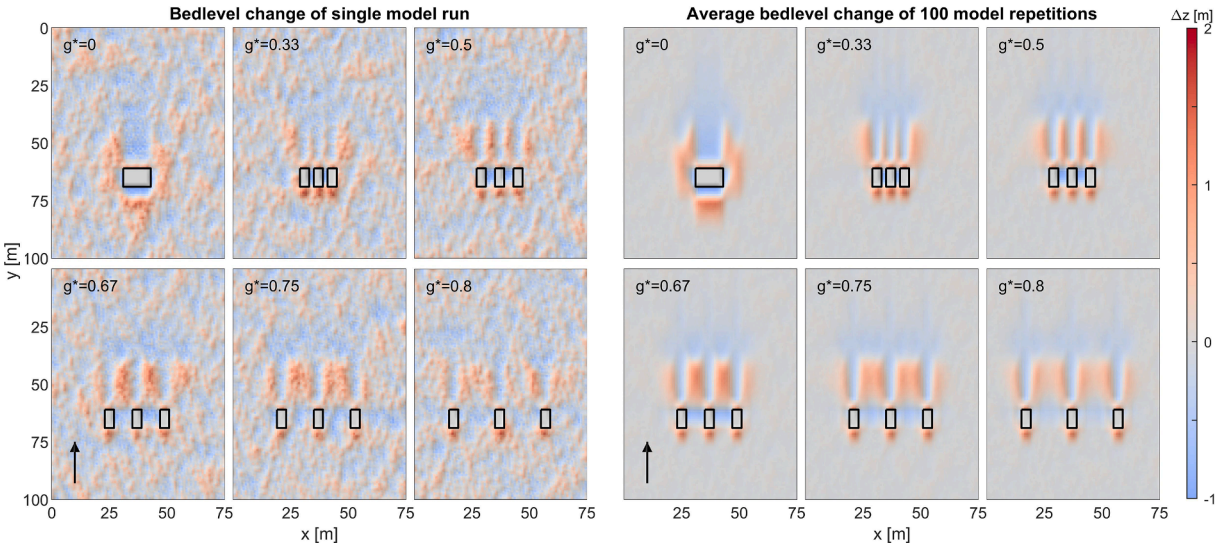

Fig. 8. Modelled deposition and erosion patterns around groups of scale models, with individual scale models 4 × 8 × 4 m (w × l × h). Building spacing is indicated by the gap ratio g*.

regime is compared to deposition and erosion patterns observed in field experiments with single buildings (section 4.1) and building groups (section 4.2). Next, the effect of a variable wind regime on short-term morphological development around buildings is examined (section 4.3). Finally, durations are extended to up to 15 years to examine interactions between natural bedform dynamics and building-induced deposition and erosion patterns (section 4.4).

Different building configurations and wind directions are examined in these scenarios (Table 1). To study the effect of building geometry, different building sizes are tested, with building widths (perpendicular to the wind) of 4, 8 and 12 m, and building lengths and heights of 4 and 8 m. To study the effect of building spacing, the set-up of the field experiment (Poppema et al., 2022c) was implemented in the model. Triplets of buildings are placed in a row perpendicular to the wind and building spacing is varied per triplet. Buildings are 4 × 8 × 4 m (w × l × h), which means that they have the same shape as the tested scale models (0.5 × 1 × 0.5 m), but have the size of actual beach cabins. This building size is chosen because it matches the cell size of the CA model: 1 × 1 m, based on the cell size for which CA model parameters have previously been calibrated (Nield and Baas, 2008; Keijsers et al., 2016). Modelling on the scale of the field experiments would require a substantial decrease in the cell size and hence a recalibration of the model parameters. Conversely, applying the scale of real buildings only increases the expected size of the deposition and erosion patterns, but not their shape, as also shown in a 5-week field experiment in which deposition and erosion around a small scale model (0.5 × 2 × 0.5 m) and a similarly shaped building (2.5 × 12 × 2.5 m) were observed simultaneously (Poppema et al., 2021).

For the scenario with different building spacings, six different building spacings are tested (Table 1). These are expressed as the gap ratio g*: the gap width relative to the combined width of the gap and building, to indicate the porosity of the set-up (Luo et al., 2014). For the wind direction scenarios, wind direction alternates deterministically, so e.g. consistently 1 iteration from the south, then 1 iteration from the west.

For the long-term scenarios, scenarios of up to 15 years are examined, with various building sizes, wind directions and building group configurations. These scenarios include larger buildings, ranging up to 25 × 25 × 15 m, to include some buildings that are larger than the developing dunes.

Results

Single buildings

The general pattern that develops around a single building in the CA model (Fig. 6) qualitatively matches the results from the field experiments quite well (Fig. 7), with deposition upwind of the building, in tails behind the building, and often some deposition next to the buildings. This is especially visible in the right half of Fig. 6, where the average of 100 model repetitions is shown to focus on consistent building-induced effects and filter out spatial and temporal variations caused by natural bedform migration. Upwind of the buildings, a deposition area develops, with a height of approximately 1.2 m, independent of building geometry. This deposition shows a steep slope toward the foot of the building, fitting field observations. The area directly against the upwind building edge initially erodes: the sediment influx into this area is lower due to upwind deposition and to slabs being diverted around the building. Where this erosion reaches the initial sediment thickness of 1 m (Fig. 6l, 6r), the local absence of further erosion decreases the downwind sediment supply. However, as the upwind deposition area becomes higher over time, slabs can also avalanche towards the building, filling up the initial erosion. For the 4 m wide buildings in Fig. 6, this results in net deposition against the upwind building edge after two years, while wider buildings still show erosion at the building edge.

Adjacent to the buildings (i.e. left and right of the buildings in Fig. 6), scour occurs, often causing erosion directly against the building walls. This scour increases with building size, with depths of 0.25 to 0.8 m. Scaled by building factor *B*, scour depth is approximately 0.06B. The area adjacent to the buildings also receives extra sand due to slabs being diverted around a building, which can also lead to extra deposition, especially in the grid cells slightly further from the building. Further downwind, beyond the building, the extra influx of sand remains while the scour stops, leading to the formation of deposition tails with heights of 0.4 to 0.9 m (approximately 0.1B). The combination of scour and deposition beside a building, followed by deposition downwind of the building, matches the patterns that formed in the field experiments (Fig. 7). In the lee behind the buildings, the very first cells usually display some accretion (0.2 to 0.5 m): the strong lee protection causes deposition of the few slabs transported over the building, while it prevents erosion. Further downwind, the low influx of sediment remains, while the lee protection slowly decreases, leading to more slabs being picked up from the bed, and hence erosion. For the field experiment with

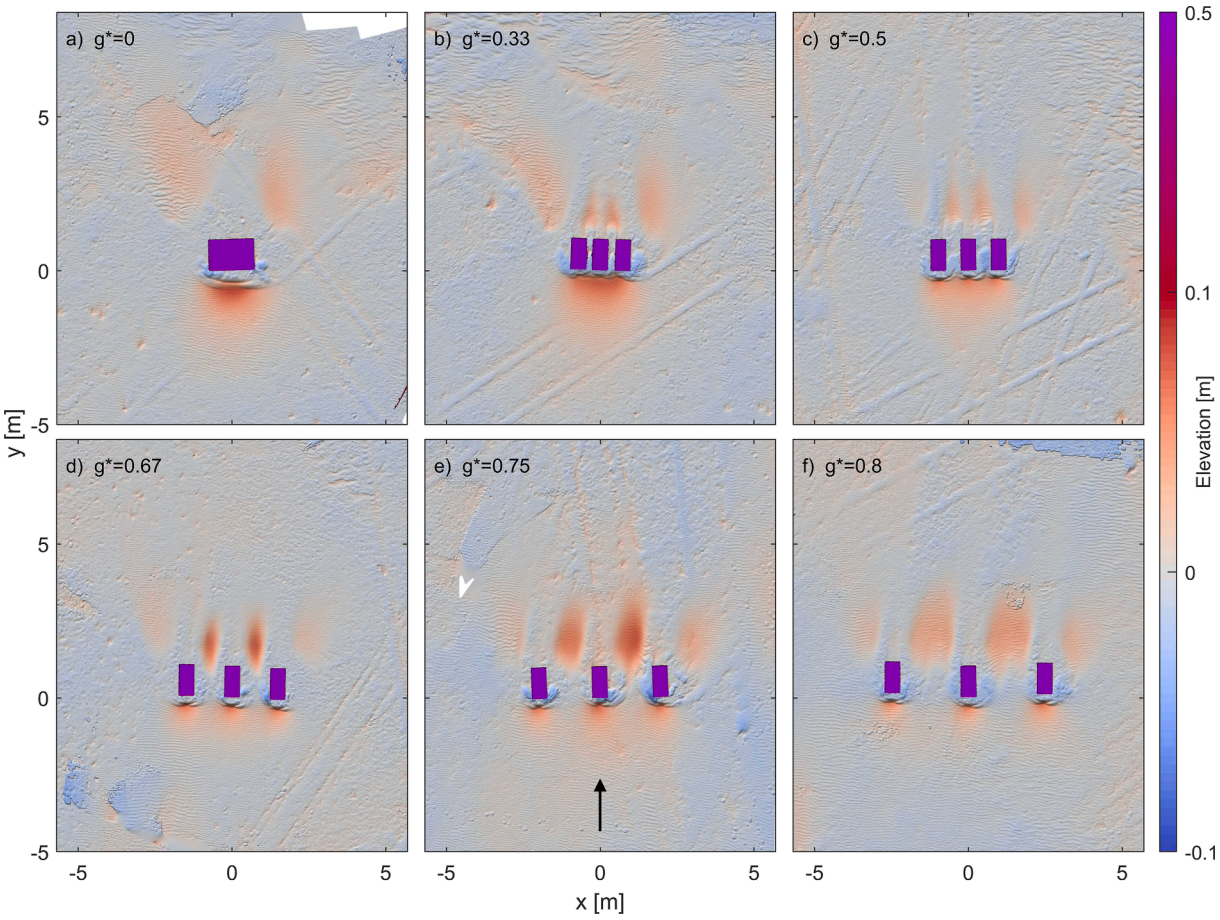

Fig. 9. Elevation maps of the scale model experiments with building groups adapted from (Poppema et al., 2022c).

Table 2
Comparison of the effect of gap width on the downwind deposition pattern around rows of buildings in the field experiment (Poppema et al., 2022c) and in the CA model.

Gap ratio	Field experiment	CA model
0.33	Inner tail is shorter and narrower than outer tail, but slightly higher.	Inner tail is narrower and lower than outer tail.
0.5	Inner tail is somewhat shorter and narrower than outer tail, but higher.	Inner tail is somewhat narrower than outer tail, but higher.
0.67	Inner tail is shorter and narrower than outer tail, but clearly higher.	Inner tail is clearly wider than outer tail, slightly higher.
0.75	Inner tail is slightly wider than outer tail and clearly higher.	Inner tail is clearly wider than outer tail, slightly higher.
0.8	Inner tail is wider and higher than outer tail. Compared to g*=0.75, inner tail is wider and lower.	Inner tails start to separate. Individual inner tails equal to outer tails.

the small scale models, this was usually not visible (see Fig. 7b and Poppema et al., 2021), but for the larger scale model placed at the beach for 5 weeks (Fig. 7a), some downwind erosion occurred.

In field experiments (Poppema et al., 2021), the length and width of the upwind deposition and the downwind depositions tails were observed to scale with building factor *B*. Upwind deposition in the field experiments had a width of approximately 2.8B, so clearly wider than the buildings. In comparison, in the CA model upwind deposition forms straight upwind of the building, as it depends on the horizon angle toward the building, and then extends a few cells to the side due to avalanching. Modelled upwind deposition length is similar to that in the experiments (2.3B), as the horizon angle at which upwind deceleration starts to occur was directly chosen based on the experiment.

The lateral and downwind deposition areas in the CA model form as a result of sediment slabs being diverted around the building. This sediment is spread to between 1 cell and a distance *B* besides the building. Hence, the width of the modelled lateral and downwind deposition increases with *B*, fitting with experimental observations. However, the quantitative effect of *B* on downwind deposition width differs: the width of the modelled deposition tails becomes somewhat larger than *B* due to avalanching spreading out the sediment, but remains well below widths of 2.5B as reached at the widest point in the field experiments. The length of the modelled tails is mostly building-independent: about 20 m, so between 2B (for the 12 × 4 × 8 m building) and 5B (the 4 × 4 × 4 m building). The field experiment showed tail length to scale with *B* and reach lengths of over 4B. This means that modelled lengths compare well to the experimental results for smaller buildings, but are clearly shorter for the larger buildings.

Multiple buildings

The general bed level dynamics around building groups (described in section 2) are captured quite well by the model. The smallest building spacing yields less downwind deposition behind the gaps than at the outside of the building group (Fig. 8). These deposition areas we refer to as inner tails resp. outer tails. As the building spacing increases, sediment transport through the gaps increases, resulting in larger inner tails and smaller outer tails. The inner tails first become both higher and wider, because both buildings next to a gap create deposition in exactly the same area. As the gap width increases further, the tails of both buildings form right next to each other, together resulting in a very wide inner tail. This agrees with the developments observed in the field

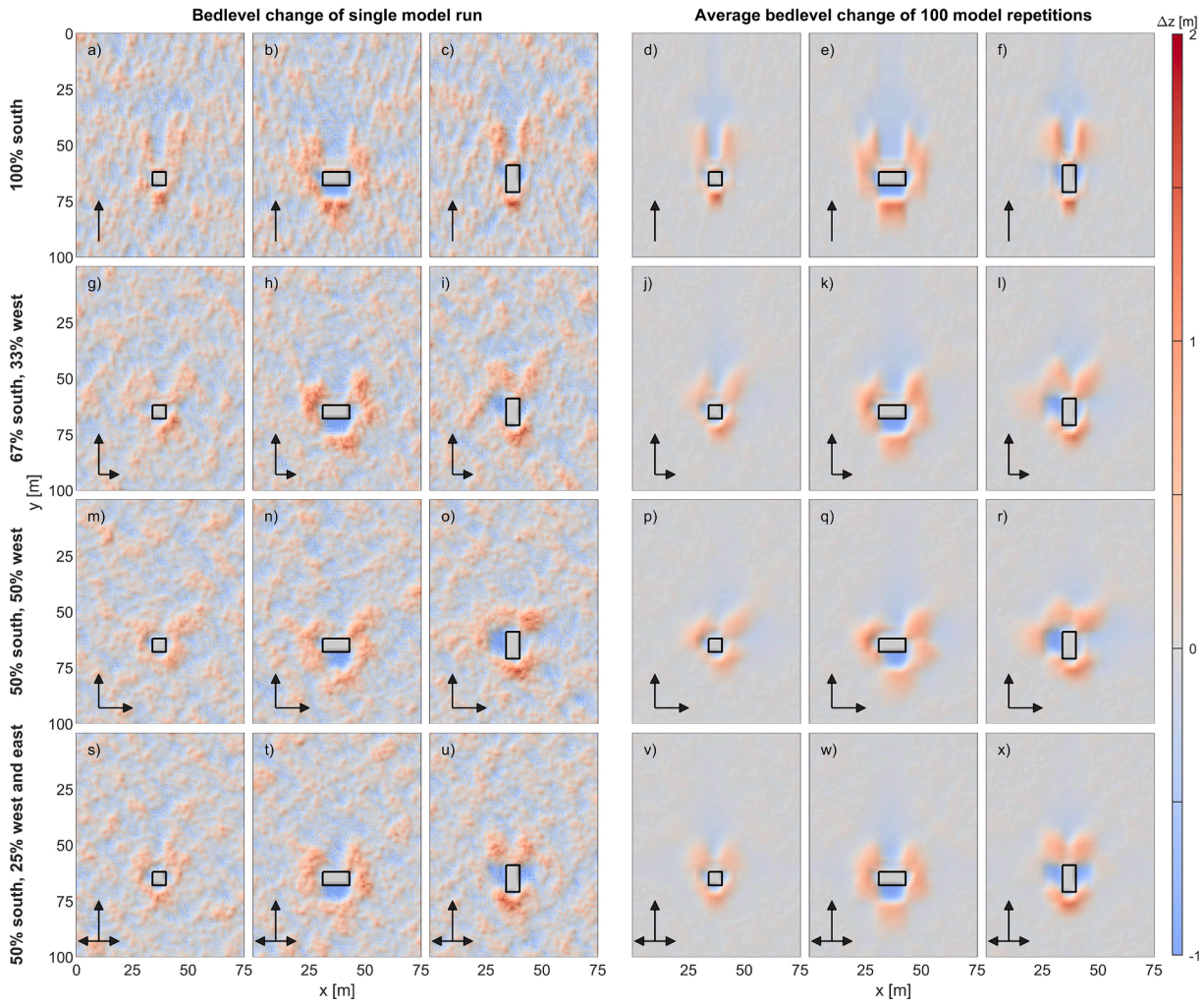

Fig. 10. Effect of different wind regimes on the topography around buildings of 6 × 6 × 6, 12 × 6 × 6 and 6 × 12 × 6 m. Y-axis labels indicate the wind regime for each row.

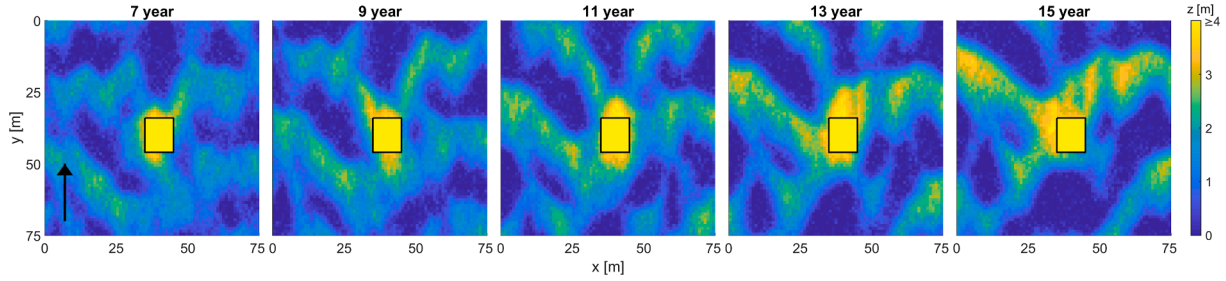

Fig. 11. Snapshots of the morphology around a building, sized 10 × 12 × 3 m, showing how a migrating bedform that arrives in front of a building (after 9 years) and migrates past the building affects deposition in the building lee. Wind is coming from below.

experiment (Fig. 9).

A more detailed comparison of the size of the inner and outer tails at all gap widths, performed in Table 2, shows some differences. Modelled inner and outer tails always have the same length: approximately 20 m, as for the individual buildings modelled before, whereas deposition length clearly showed variation in the field experiments. The underestimation of the deposition tail length results in relatively wide and short inner tails at the largest gap widths (17 × 22 m, so 4B × 5.5B), whereas the field experiment showed tails that were clearly longer than they were wide (1.6 × 3.6 m, so 3B × 7B). In addition, some transitions between deposition topologies occur at a smaller gap ratio (g*) in the CA model than in the field experiment. This is the case for the gap ratio at which the inner tail becomes wider than the outer tail (g*=0.75 vs 0.5) and for the gap ratio at which the inner tail can be recognized as consisting of two adjacent tails from two buildings (g*=0.75 vs 0.8).

Wind direction

Next, we use the CA model to examine the effects of multi-directional wind regimes. Again initial bed level change is examined, so after a period of 2 years (Fig. 10). For a unidirectional wind from the south, the resulting deposition patterns are symmetrical, with two deposition tails

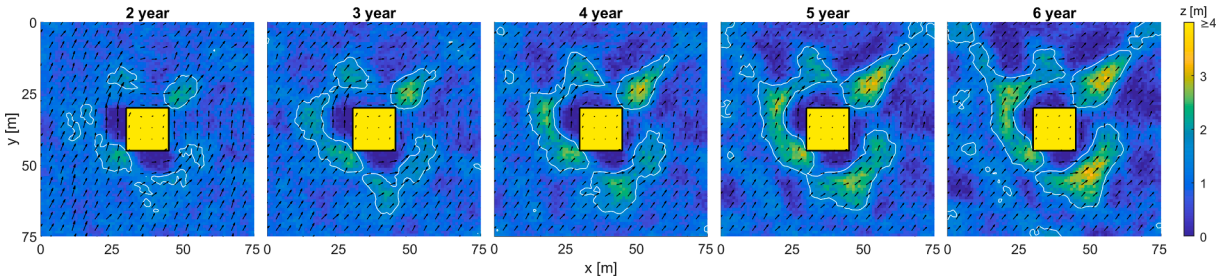

Fig. 12. Snapshots of the morphology around a building, sized 15 × 15 × 6 m and the annual sediment transport pattern. White lines indicate the 1.5 m contour line. Black arrows indicate the flow pattern of sand slabs, averaged over 1 year. The wind regime is 50 % south, 50 % west.

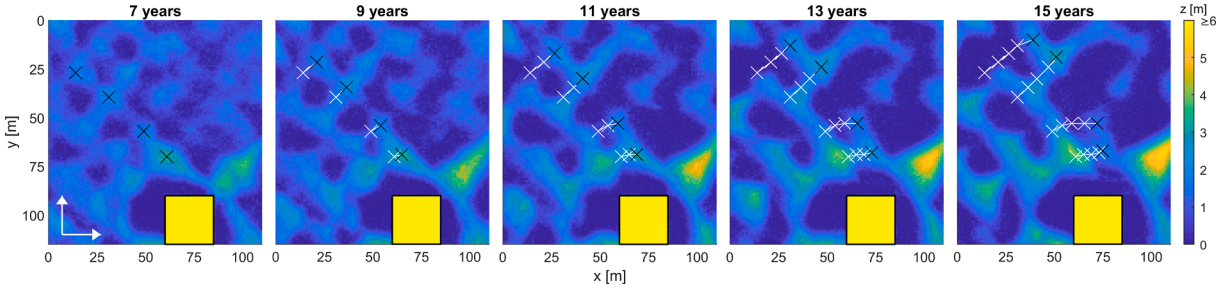

Fig. 13. Snapshots of the morphology around a building, sized 25 × 25 × 15 m. The location of the crest of four dunes is indicated to emphasize the migration direction in the lee protection zone downwind of a building. Black crosses indicate the dune location in the current snapshot, white crosses the location of the previous snapshots. The wind regime is 50 % south, 50 % west.

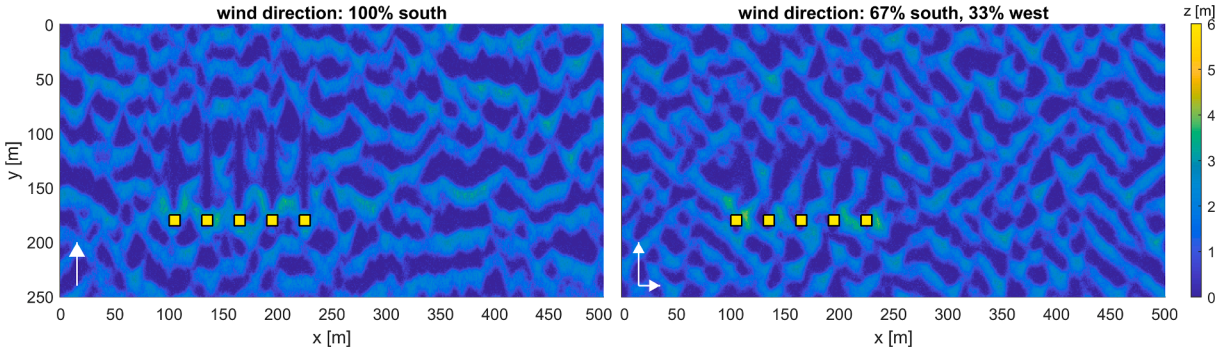

Fig. 14. The morphological development after 12 years, around a row of 5 buildings of 10 × 10 × 6 m with gaps of 20 m between buildings and for two different wind regimes.

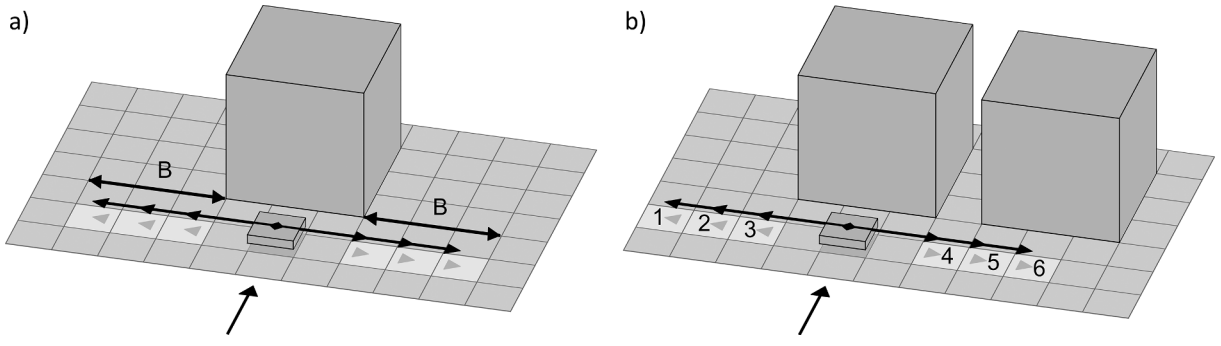

Fig. 15. A slab in transport upwind of a building. If this slab is moved sideward, it is shifted to a random cell in of the destination area, i.e. the lighter coloured cells of the same grid row (the same distance upwind of the building), at between 1 cell and a distance *B* to the side of the building. Cell numbers are referred to in the text.

of equal length. If the wind regime changes to bidirectional, from the south and west, the sediment dynamics and deposition pattern change. At the southern wall, transport to the north (during southern wind) is impeded by upwind deceleration, while transport to the east (during western wind) is increased by lateral scour. Conversely, at the eastern wall, transport to the north is increased by scour, while transport to the

east is limited by the lee protection. The same processes occur at the western and northern wall. As a result sand is redirected around the building to the north-east corner.

For a square building and wind regime that is 50 % south, 50 % west, this leads to a diagonally oriented deposition tail at the northeast corner and symmetrical pattern around the southwest-northeast axis (Fig. 10p). Upwind deposition, which occurs at the southern and western wall, is blown to the eastern respectively northern end of these walls, limiting deposition at the south-west upwind corner. Instead deposition collects at the south-east and north-west corner, where it forms lee protection zones to the east (during western wind) and to the north (during southern wind), making the areas grow to the northeast.

If the building is rectangular instead of cubic, the larger building factor B in one direction causes upwind deposition in that direction to occur further from the building. This happens for instance at the southern wall in Fig. 10q, where the peak of the deposition lies 11 m from the building, compared to 6 m at the western wall. Scaled by the building factors B (9.5 m resp. 6 m for each wind direction), this amounts to 1.15B and 1B, so approximately equal. In addition, the deposition areas at the northeast and northwest corner are more clearly separated than in subplot p due to the larger distance between these corners. If the wind regime is 67 % south, 33 % west (subplot j), the resulting topography lies between the results for a 50%-south-50%-north regime and a unidirectional wind regime: two deposition tails develop, with the largest deposition tail at the northeast downwind corner, oriented to the north-northeast.

For a wind regime with 50 % southern, 25 % western and 25 % eastern wind, the morphology develops similarly to that of a fully southern wind. However, the eastern and western wind spread out sediment to the east and west, while the sediment transport rate to the north is lower. This results in a pattern that is smeared out east–west, with especially the deposition tails becoming shorter but wider.

Long-term interactions

To explore the interactions between buildings and natural bedform dynamics, dynamics over a longer period and with a larger building are examined. Fig. 11 shows how the morphological development around a building is affected by bedform dynamics in the surrounding area, with wind unidirectional from the south. After 9 years, a dune is present directly upwind of the building, reaching an elevation of 3.5 m. This decreases the horizon angle towards the building, which in turn decreases sideward slab transport around the building and increases transport over the building. As a result, strong deposition occurs in the lee protection zone behind the building, which reaches slightly higher than the building (4.3 m after 11 years) and clearly surpasses the height of bedforms unaffected by the building. After 13 years, the dune in front of the building disappears. This decreases sediment transport over the building, which causes the deposition area in the lee to become smaller (with a maximum elevation of 3.5 m after 15 years).

Natural bedform dynamics are also affected by buildings. Fig. 12 shows a building shaping the location and direction of bedform growth. It presents the annual slab transport around a building as well as the bedform development for a bidirectional wind regime, with wind direction alternating equally between south and west. The transport pattern shows the redirection of sediment around a building, as explained before (section 4.3). The 1.5 m elevation contour shows that bedform migration and evolution follow this pattern. For instance, the deposition initially present at the south-eastern corner shows diagonal development south of the building, but east of the building it deviates from the average wind direction and grows to the north.

Looking at even larger buildings and time spans of up to 15 years, dune migration is affected in an even wider area of influence. In Fig. 13, the migration of four dune crests is indicated, for the same bidirectional wind regime as Fig. 12. The building here is 25 × 25 × 15 m, such that the building is wider than the dunes and can affect (the horizon angles of) all dune cells simultaneously. The dune crests initially form a straight line, and without a building these sand dunes would all migrate in the average wind direction, so diagonally to the north-east. The dunes furthest from the building indeed migrate north-east, but the dunes closer to the building migrate to the east, because their northward migration is decelerated by the lee protection behind the building, while the eastward migration is accelerated by lateral scour.

Finally, we examine how a group of buildings affects bedform development over a larger area (Fig. 14). For a unidirectional wind from the south, transverse dunes develop in the area without buildings, at the right side of the domain. The building group at the left locally causes increased deposition, which decreases the sediment transport to the area downwind of the buildings. As a result of the lower sediment supply, barchan dunes instead of transverse dunes develop in this area. For a bidirectional wind regime (67 % south, 33 % west), the area without buildings develops a dune topology resembling star dunes, i.e. a grid of dunes oriented perpendicular and parallel to the mean wind direction. Behind the buildings, the deposition tails grow to the north, in a manner similar to linear dunes and reaching lengths of 50 m.

Discussion

The new CA rules for sediment dynamics around buildings replicate observed deposition and erosion patterns around buildings qualitatively well. They result in a realistic flux pattern around obstacles (Fig. 5). Moreover, the modelled shape of the morphological patterns around single buildings and building groups is comparable to that observed in field experiments. Quantitative comparison between CA model results and field experiments shows that modelled deposition around buildings is often smaller than observed deposition in field experiments. This is particularly notable for the upwind deposition width. In addition, the downwind deposition length is almost independent of building size in the CA model, whereas it increased with building width and height in the field.

These discrepancies partly follow from differences between field conditions and the cellular automaton environment. In the field, the wind direction fluctuates, whereas the CA model has a constant wind direction (or orthogonal variations). Slightly oblique winds that occur in the field can disperse sediment, causing deposition and erosion patterns to become wider. This also matches the CA simulation with 50 % western wind and 25 % northern and southern wind, which shows deposition tails that are slightly wider than for unidirectional wind. In addition, field experiments and the CA model differ in building size. The CA simulations replicate real building sizes rather than the smaller scale models because of the cell size at which DECAL was calibrated (Nield and Baas, 2008). The duration of the CA simulations was also longer. First, the longer duration follows from deposition taking more time to develop for large buildings than for small scale models. Second, the field experiments were by design performed on days with abundant sediment transport, whereas DECAL and all derivative CA models employ a constant sediment flux and weekly to monthly timesteps (Baas, 2002; Keijsers et al., 2016) to model average long-term evolution.

Discrepancies partly result from the new model rules simplifying the complex processes around a building. They capture the general morphological dynamics around buildings well, including the shape of the deposition and erosion patterns, interactions between multiple buildings and feedback effects over time with natural dune dynamics. These rules are based on the horizon angle in the four cardinal directions. So cells that are not horizontally or vertically in line with a building are not directly affected, apart from some grid cells receiving sideward sediment transport. Hence the probability of deposition and erosion at the deposition tails, obliquely downwind of a building, are *not* changed by the building. Instead, deposition tails form due to a surplus of sediment transport, persisting from the obliquely upwind cells having received sideward sediment transport. The distance over which this surplus decays, and hence the initial deposition tail length, depends on

the deposition probability p_d. In reality, this deposition is also aided by horizontal flow convergence in the horseshoe vortex tails (Pourteimouri et al., 2022).

The choice for idealized horizon-angle-based rules, without including all details of building effects, is linked to the nature of the CA model. The model rules do not specifically enforce effects around buildings. Instead, universally applicable rules evaluate the horizon angle throughout the entire domain in order to change the local sediment transport. This leads to *self-organizing* behaviour, where the morphological impact of a building emerges as the combined effect of all model rules. However, for a more precise quantitative replication of the morphological effects of specific buildings, locally *forced* building effects might need to be explicitly defined in addition to the general domain-wide rules currently used.

This means that the general horizon-angle-based rules fit the objective of this study, to explore possible interactions between building-induced morphological patterns and self-organized aeolian bedform dynamics. The success in simulating general morphological dynamics around buildings makes the model suitable to obtain insights on mechanisms of how building effects and natural dune dynamics interact. For example, the model helps to understand how sediment collecting around buildings affects downwind sediment transport and dune topology. When desired, such simulations can even be performed in a scenario study or sensitivity analysis, thanks to the relatively low computational cost (e.g. the 12-year simulation of Fig. 14 takes 5 min[1]).

The general horizon-based rules might also be applicable to other processes and environments. The flow recirculation and deceleration that occur in front of buildings can also be found in natural environments that have steep slopes. They occur at cliffs that border beaches (Tsoar and Blumberg, 1991), steep dune scarps created by storms (Nishi et al., 1995; George et al., 2021), or foredunes with steep slopes that hamper landward sediment transport (Christiansen and Davidson-Arnott, 2003). In addition, horizon angles could offer an elegant mechanism to change the modelled steepness of the stoss slope of dunes, which tends to be quite high in the Werner and DECAL algorithm (Momiji et al., 2000). Moreover, the examined building-bedform interaction shows strong parallels to the interaction of marine sand waves with fixed structures such as pipelines (Morelissen et al., 2003), indicating opportunities to apply these rules in subaqueous environments.

There are some limitations stemming from the chosen model rules. The rules assume a steep upwind slope creates sediment transport *around* an obstacle. This is only true for obstacles of limited width. However, for relatively wider buildings, airflow increasingly flows *over* instead of *around* the building, until, at an aspect ratio (w/h) of about 10, the flow fundamentally changes, with additional vortices over the building breaking up the simple horseshoe vortex structure (Martinuzzi and Tropea, 1993). Hence the model should not be applied to very wide buildings. In addition, the current algorithm for determining the obstacle width looks for the number of consecutive neighbouring cells, perpendicular to the wind direction, with at least the same elevation. This works well for wind perpendicular to the building. However, for oblique wind directions this algorithm would have to be adapted.

Oblique wind directions were examined in the model with wind alternatingly coming from the south and the west, so on average diagonal to the building. However, this is not the same as an oblique wind direction in the field. In the CA model, this alternating wind results in a single deposition tail behind the downwind building corner (Fig. 10). In the field experiments (Poppema et al., 2022c), wind consistently blowing obliquely to a building creates the usual horseshoe deposition with two tails, instead of forming a singe deposition tail behind the downwind corner. This also shows that the net sediment transport direction and average wind direction do not necessarily coincide. If buildings or dunes are present, they can shelter the bed during specific wind directions, such that wind is decelerated, while wind is unaffected or even accelerated during other wind directions. As a result, the net sediment transport direction around obstacles, being manmade buildings or natural bedforms such as dunes, can differ from the average or dominant wind direction.

[1] With a grid size of 650×400 cells and 50 aeolian iterations per year, run on an Intel i7-8750H hexacore CPU.

Conclusion

In this study, we examined how building-induced deposition and erosion patterns interact with self-organized aeolian bedform dynamics. Novel cellular automaton rules were developed to characterize sediment transport around bluff obstacles such as buildings. The rules use the horizon angle in the four cardinal directions to describe the acceleration and deceleration of sediment around obstacles, as well as sideward transport around obstacles. These general rules, which are applied throughout the entire model domain to both sandy cells and buildings, result in self-organizing behaviour that creates natural dune formation, but also patterns of deposition and erosion around bluff objects such as buildings. Combined, the rules give rise to a realistic sediment flux pattern around buildings. Comparison of model results to field experiments show that the modelled morphological development around buildings is realistic in terms of the shape of deposition and erosion patterns, as well as the interactions that occur around rows of buildings. However, some quantitative differences exist between the field experiments and model results. Especially downwind deposition tails are shorter in the CA results than in the field experiment, and do not show the desired dependency on building dimensions.

With this model, the effect of buildings on their environment and interactions with natural bedform dynamics can be studied. This is especially relevant for coastal settings where dunes need to have a certain height or volume for protection against flooding. In addition, there are broader applications to the new rules, as sediment dynamics in front of steep slopes are also important for natural cliffs or dune scarps created by storm erosion.

The simulations performed in this study showed interactions between local building-induced effects and natural aeolian bedform dynamics. The local morphological pattern around buildings responds to the bedform dynamics in their surroundings, with modelled deposition in the lee behind buildings increasing when a migrating sand dune is temporarily located in front of a building. Conversely, buildings also affect bedform dynamics in their surroundings. By diverting sediment around a building, the lee behind buildings receives less sediment, while sediment transport next to a building increases. For multi-directional wind regimes, sediment is redirected around a building. By providing shelter against the wind in a specific direction, buildings can steer sediment transport in their surroundings, and thereby steer the location and direction of dune growth. Larger buildings can hereby also change the dune migration trajectory. In essence, this means the local *net* sediment transport direction around buildings can diverge from the *average* wind direction.

CRediT authorship contribution statement

Daan W. Poppema: Methodology, Investigation, Formal analysis, Writing – original draft, Writing – review & editing. **Andreas C.W. Baas:** Conceptualization, Methodology, Writing – review & editing. **Suzanne J.M.H. Hulscher:** Writing – review & editing, Supervision. **Kathelijne M. Wijnberg:** Conceptualization, Supervision, Writing – review & editing, Project administration, Funding acquisition.

Declaration of Competing Interest

The authors declare that they have no known competing financial interests or personal relationships that could have appeared to influence the work reported in this paper.

Data availability

Data will be made available on request.

Acknowledgements

This research forms part of the ShoreScape project. It is funded by the Netherlands Organization for Scientific Research (NWO), contract number ALWTW.2016.036, co-funded by Hoogheemraadschap Hollands Noorderkwartier and Rijkswaterstaat, and in kind supported by Deltares, Witteveen&Bos, and H + N + S.

Appendix:. Detailed description CA rules for buildings

The representative downwind horizon angle

The CA model uses the *representative* downwind horizon angle to include the effect of both obstacle width and height. For the CA implementation, the model first determines for every cell which downwind cell causes the horizon angle, i.e. which cell touches the imaginary horizon line. The obstacle height is equal to the height difference Δh between both cells, while obstacle width w is determined from the number of consecutive neighbouring cells perpendicular to the wind direction that have at least the same elevation as the horizon-causing cell (Fig. 3). This gives building factor B and distance Δx between both cells, which allows for calculating the representative downwind horizon angle $\alpha_{rep,\ downw}$ (eq. 1–4). In the calculation, the aspect ratio (w/h-ratio) of the buildings is limited to range between 0.2 and 4 (Poppema et al., 2021), because for very tall or very wide buildings, the smaller building dimension becomes increasingly dominant for the size of airflow patterns (Martinuzzi and Tropea, 1993) and the resulting morphological patterns.

$$w = \min(w, 4{\cdot}\Delta h) \tag{1}$$

$$\Delta h = \min(\Delta h, w/0.2) \tag{2}$$

$$B = \begin{matrix} w^{2/3}{\cdot}\Delta h^{1/3}, & \Delta h \geq 0 \\ 0, & \Delta h < 0 \end{matrix} \tag{3}$$

$$\alpha_{rep,downw} = \tan^{-1}\left(\frac{B}{\Delta x}\right) \tag{4}$$

Upwind deposition

The representative horizon angle ($\alpha_{rep,\ downw}$) affects the erosion and deposition probabilities through the *upwind deposition effectiveness* (η_{upw}), following the curve shown in Fig. 4a. Deposition, and hence η_{upw}, start to increase at a representative horizon angle of about 20°, based on upwind deposition in field experiments (Poppema et al., 2021) starting at a distance of approximately 2.3B from the building. This also fits with observations of sediment transport being able to traverse mildly sloping dune fronts, while forming dune ramps (i.e. upwind deposition) at dunes steeper than approximately 20° (Christiansen and Davidson-Arnott, 2003) and with the limited sediment transport over such steep foredunes observed by Arens et al. (1995) and Bauer et al. (2012). Maximum upwind deposition effectiveness occurs at 55°, based on our observation (Poppema et al., 2021) that the crest of the upwind deposition occurs at a distance of 0.78B from buildings (using $\tan^{-1}\frac{1}{0.78}$). The maximum deposition effectiveness is set to 25 % to allow for sediment transport past a building, as deposition and sediment transport behind buildings show that transport over a building is not zero. Directly in front of a building, there is little deposition or even erosion as the strong airflow blows most sand around a building, so the deposition effectiveness returns to zero at a horizon angle of at 90°.

Lateral scour

Airflow is only accelerated in the proximity of buildings, so a minimum lateral horizon angle is required before scour occurs. The same value is used as for the upwind deposition: 20°. At $\alpha_{lat} = 180^{\circ}$, $\eta_{lat} = -1$, so peak scour effectiveness is reached at the maximum possible horizon angle, which approaches 180° for a cell in between two very tall buildings. For $20^{\circ} < \alpha_{lat} \leq 180^{\circ}$, p_e and p_d depend quadratically on the horizon angle (Fig. 4b). The quadratic interpolation is applied because airflow returns faster to the undisturbed conditions perpendicular to the wind direction than in the wind direction, and hence scour is concentrated closer to a building than upwind or downwind deposition.

Lee protection zone

Previous CA models implemented the effect of obstacles sheltering the bed in their lee as shadow zones, so zones with full deposition ($p_d = 1$) and no erosion ($p_e = 0$) in all cells with an upwind horizon angle of more than 15° (Baas, 2002; Keijsers, 2015). This means that for a cell size of 1 m, a shadow zone forms as soon as a cell is 30 cm lower than the previous cell. In more physical terms, a bedform of 30 cm high would catch all aeolian sediment transport over it, so streamers cannot pass it (within a single aeolian iteration). In practice, such small bedforms would only catch a part of the sediment transport over a cell. For a larger dune most sediment would indeed deposit in its lee, but this sediment would still not all deposit in the very first cell behind a dune. In case of natural dune systems, these inaccuracies of binary shadow zones are mitigated by bedforms migrating constantly, spreading out deposition on the long term, even if it is too concentrated in a single iteration. However, buildings have a fixed position and a substantial height difference with their surroundings, making it more important to implement a more realistic and gradual sheltering mechanism. Therefore, a gradual *lee protection effectiveness* replaces the old binary shadow zones, with zero effectiveness if the upwind horizon angle is 0°, 100 % at

45° or more and linearly interpolated effectiveness in between (Fig. 4c).

The full lee protection effectiveness for horizon angles larger than 45° denotes the recirculation zone, in which the wind direction is reversed, causing full deposition of incoming slabs at the start of the recirculation zone. The 45° value is chosen because the length of the recirculation zone is approximately equal to the obstacle height, for obstacles that are similar in height and width (Wilson, 1979). The lee protection effectiveness is affected up to horizon angles of 0° due to the persistence of the velocity deficit in the wake of obstacles. After the reattachment point the local wind *direction* matches the undisturbed wind direction again, but the wind *velocity* remains lower. This velocity deficit can persist very far behind obstacles, and has been observed 30 obstacle heights behind a building (Peterka et al., 1985), which is equivalent to an upwind horizon angle of about 2°. In the CA model, the lee protection effectiveness nevertheless applies to upwind horizon angles ranging between 0° and 45°, where effectively the 0°angle will not occur because there will always will be some self-organized bedforms developing.

Sideward sediment transport

Directly upwind of a building, a rolling vortex blows sand against the general wind direction, creating the (crest of the) upwind deposition area, while simultaneously transporting sand to the side, around the building. In field experiments (Poppema et al., 2021), the crest of the upwind deposition is observed at a distance of approximately 0.78B from the building ($B = w^{2/3}h^{1/3}$), fitting quite well with the aerodynamic upwind separation distance of $0.7\sqrt{wh}$ as reported by Beranek (1984). Because experiments (Beranek, 1984; Martinuzzi and Tropea, 1993) and numerical modelling (Thiis and Jaedicke, 2000; Gao and Chow, 2005) show that streamlines already start to deflect to the side before the upwind separation point is reached, a slightly larger distance of 1B is employed as the starting distance for sideward sediment transport. This results in a minimum required representative horizon angle ($\alpha_{rep,downw}$) of 45°. In cells where $\alpha_{rep,downw} > 45^{\circ}$, the probability of sideward transport is set to 50 %, to keep a portion of the sediment flux available for further downwind transport, thereby allowing for some deposition closer to the building, and a small sediment flux over the building.

To determine *to which cell* sidewards transported slabs are shifted, scaling length B is used once more. The vortex in front of the building, with a diameter proportional to B, is wrapped around the building. So it transports sediment to at most a distance B next to the building. Therefore, a sidewards shifted slab is shifted to a cell that is between 1 cell and a distance B (rounded to an integer number of cells) at either side of a building (Fig. 15a). The actual cell where a slab is transported to is selected randomly from this destination area.

The mechanism of randomly selecting one of the cells from the destination area is designed to also model situations with multiple buildings. For a single building oriented perpendicular to the wind, this mechanism results in an (on average) even distribution of sediment between both building sides. For a row of adjacent buildings with a building spacing smaller than B, this changes. Let us assume a slab in transport upwind of a building group as sketched in Fig. 15b. If the slab is shifted sideward to a grid column in front of the gap or outside of the building group (cell 1, 2 3 or 4 in Fig. 15b), the slab will remain in this column. However, if the slab is placed upwind of a neighbouring building (cell 5 or 6), it can be subject to sideward transport again in the next row. This effectively entails a repeated possibility for sideward slab transport to the outside of a building group, resulting in increased sediment transport around a building group and decreased sediment transport trough the gaps. This fits the results of wind tunnel and field experiments with a row of buildings, (Luo et al., 2014; Poppema et al., 2022c), in which a small building spacing resulted in smaller deposition areas behind the gaps than at the outside of a group.

References

Abbasi, H.R., Opp, C., Groll, M., Rohipour, H., Gohardoust, A., 2019. Assessment of the distribution and activity of dunes in Iran based on mobility indices and ground data. Aeolian Res. 41, 100539 https://doi.org/10.1016/j.aeolia.2019.07.005.

Arens, S.M., Van Kaam-Peters, H.M.E., Van Boxel, J.H., 1995. Air flow over foredunes and implications for sand transport. Earth Surf. Proc. Land. 20 (4), 315–332. https://doi.org/10.1002/esp.3290200403.

Baas, A.C.W., 2002. Chaos, fractals and self-organization in coastal geomorphology: simulating dune landscapes in vegetated environments. Geomorphology 48 (1), 309–328. https://doi.org/10.1016/S0169-555X(02)00187-3.

Baas, A.C.W., 2007. Complex systems in aeolian geomorphology. Geomorphology 91 (3), 311–331. https://doi.org/10.1016/j.geomorph.2007.04.012.

Bagnold, R.A., 1941. The Physics of Blown Sand and Desert Dunes. Chapman & Hall, Londen.

Barchyn, T., Hugenholtz, C.H., 2012. A new tool for modeling dune field evolution based on an accessible, GUI version of the Werner dune model. Geomorphology 138 (1), 415–419. https://doi.org/10.1016/j.geomorph.2011.09.021.

Bauer, B.O., Davidson-Arnott, R.G.D., Walker, I.J., Hesp, P.A., Ollerhead, J., 2012. Wind direction and complex sediment transport response across a beach–dune system. Earth Surf. Proc. Land. 37 (15), 1661–1677. https://doi.org/10.1002/esp.3306.

Beranek, W.J., 1984. Wind environment around single buildings of rectangular shape. Heron 29 (1), 4–31.

Beyers, M., Waechter, B., 2008. Modeling transient snowdrift development around complex three-dimensional structures. J. Wind Eng. Ind. Aerodyn. 96 (10–11), 1603–1615. https://doi.org/10.1016/j.jweia.2008.02.032.

Bruno, L., Horvat, M., Raffaele, L., 2018. Windblown sand along railway infrastructures: A review of challenges and mitigation measures. J. Wind Eng. Ind. Aerodyn. 177, 340–365. https://doi.org/10.1016/j.jweia.2018.04.021.

Christiansen, M. B., & Davidson-Arnott, R. (2003). *Effects of dune ramps on sediment supply to coastal foredunes: Skallingen, SW Denmark.* Paper presented at the International conference on coastal sediments 2003.

Cooke, R.U., Warren, A., Goudie, A.S., 1993. Desert geomorphology. CRC Press.

De Groot, A. V., Berendse, F., Riksen, M., Baas, A., Slim, P. A., Van Dobben, H. F., & Stroosnijder, L. (2011). *Modelling coastal dune formation and associated vegetation development.* Paper presented at the EGU 2011, Vienna, Austria.

Dong, Z., Liu, X., Wang, H., Zhao, A., Wang, X., 2003. The flux profile of a blowing sand cloud: a wind tunnel investigation. Geomorphology 49 (3), 219–230. https://doi.org/10.1016/S0169-555X(02)00170-8.

Duran, O., Moore, L.J., 2013. Vegetation controls on the maximum size of coastal dunes. Proc Natl Acad Sci U S A 110 (43), 17217–17222. https://doi.org/10.1073/pnas.1307580110.

Eastwood, E., Nield, J., Baas, A., Kocurek, G., 2011. Modelling controls on aeolian dune-field pattern evolution. Sedimentology 58 (6), 1391–1406. https://doi.org/10.1111/j.1365-3091.2010.01216.x.

Fonstad, M.A., 2013. Cellular Automata in Geomorphology. Treatise on Geomorphology 2, 117–134. https://doi.org/10.1016/B978-0-12-374739-6.00035-X.

Galiforni Silva, F., Wijnberg, K.M., de Groot, A.V., Hulscher, S.J.M.H., 2018. The influence of groundwater depth on coastal dune development at sand flats close to inlets. Ocean Dyn. 68 (7), 885–897. https://doi.org/10.1007/s10236-018-1162-8.

Galiforni Silva, F., Wijnberg, K.M., de Groot, A.V., Hulscher, S.J.M.H., 2019. The effects of beach width variability on coastal dune development at decadal scales. Geomorphology 329, 58–69. https://doi.org/10.1016/j.geomorph.2018.12.012.

Gao, Y., Chow, W.K., 2005. Numerical studies on air flow around a cube. J. Wind Eng. Ind. Aerodyn. 93 (2), 115–135. https://doi.org/10.1016/j.jweia.2004.11.001.

George, E., Lunardi, B., Smith, A., Lehner, J., Wernette, P., Houser, C., 2021. Short communication: Storm impact and recovery of a beach-dune system in Prince Edward Island. Geomorphology 384, 107721. https://doi.org/10.1016/j.geomorph.2021.107721.

Hernández-Calvento, L., Jackson, D.W.T., Medina, R., Hernández-Cordero, A.I., Cruz, N., Requejo, S., 2014. Downwind effects on an arid dunefield from an evolving urbanised area. Aeolian Res. 15, 301–309. https://doi.org/10.1016/j.aeolia.2014.06.007.

Hesp, P.A., 1981. The formation of shadow dunes. J. Sediment. Petrol. 51 (1), 101–112. https://doi.org/10.1306/212F7C1B-2B24-11D7-8648000102C1865D.

Hoonhout, B.M., De Vries, S., 2016. A process-based model for aeolian sediment transport and spatiotemporal varying sediment availability. J. Geophys. Res. Earth Surf. 121 (8), 1555–1575. https://doi.org/10.1002/2015JF003692.

Hoonhout, B.M., Van Thiel de Vries, J., 2013. Invloed van strandbebouwing op zandverstuiving, Adviezen voor vergunningverlening. Deltares, Delft.

Hunt, J., 1971. The effect of single buildings and structures. Phil. Trans. R. Soc. Lond. A 269 (1199), 457–467. https://doi.org/10.1098/rsta.1971.0044.

Iversen, J.D., Wang, W.-P., Rasmussen, K.R., Mikkelsen, H.E., Hasiuk, J.F., Leach, R.N., 1990. The effect of a roughness element on local saltation transport. J. Wind Eng. Ind. Aerodyn. 36, 845–854. https://doi.org/10.1007/978-3-7091-6703-8_5.

Jackson, N.L., Nordstrom, K.F., 2011. Aeolian sediment transport and landforms in managed coastal systems: A review. Aeolian Res. 3 (2), 181–196. https://doi.org/10.1016/j.aeolia.2011.03.011.

Keijsers, J.G.S., 2015. Modelling foredune dynamics in response to climate change. Wageningen University. Doctoral thesis),.

Keijsers, J.G.S., De Groot, A.V., Riksen, M.J.P.M., 2016. Modeling the biogeomorphic evolution of coastal dunes in response to climate change. J. Geophys. Res. Earth Surf. 121 (6), 1161–1181. https://doi.org/10.1002/2015jf003815.

Lorenz, R.D., Gasmi, N., Radebaugh, J., Barnes, J.W., Ori, G.G., 2013. Dunes on planet Tatooine: Observation of barchan migration at the Star Wars film set in Tunisia. Geomorphology 201, 264–271. https://doi.org/10.1016/j.geomorph.2013.06.026.

Luo, W., Dong, Z., Qian, G., Lu, J., 2012. Wind tunnel simulation of the three-dimensional airflow patterns behind cuboid obstacles at different angles of wind incidence, and their significance for the formation of sand shadows. Geomorphology 139, 258–270. https://doi.org/10.1016/j.geomorph.2011.10.027.

Luo, W., Dong, Z., Qian, G., Lu, J., 2014. Near-wake flow patterns in the lee of adjacent obstacles and their implications for the formation of sand drifts: a wind tunnel simulation of the effects of gap spacing. Geomorphology 213, 190–200. https://doi.org/10.1016/j.geomorph.2014.01.008.

Luo, W., Lu, J., Qian, G., Dong, Z., 2016. Influence of the gap ratio on variations in the surface shear stress and on sand accumulation in the lee of two side-by-side obstacles. Environmental Earth Sciences 75 (9), 766. https://doi.org/10.1007/s12665-016-5588-3.

Malvarez, G., Jackson, D., Navas, F., Bilbao, I., Hernández-Calvento, L., 2013. A Conceptual Model for Dune Morphodynamics of the Corralejo Dune System. Fuerteventura Spain (Vol. SI 65). https://doi.org/10.2112/SI65-260.1.

Martinuzzi, R., Tropea, C., 1993. The Flow Around Surface-Mounted, Prismatic Obstacles Placed in a Fully Developed Channel Flow (Data Bank Contribution). J. Fluids Eng. 115 (1), 85–92. https://doi.org/10.1115/1.2910118.

McKenna Neuman, C., Bédard, O., 2015. A wind tunnel study of flow structure adjustment on deformable sand beds containing a surface-mounted obstacle. J. Geophys. Res. Earth Surf. 120 (9), 1824–1840. https://doi.org/10.1002/2015jf003475.

McKenna Neuman, C., Sanderson, R.S., Sutton, S., 2013. Vortex shedding and morphodynamic response of bed surfaces containing non-erodible roughness elements. Geomorphology 198, 45–56. https://doi.org/10.1016/j.geomorph.2013.05.011.

Momiji, H., Carretero-González, R., Bishop, S.R., Warren, A., 2000. Simulation of the effect of wind speedup in the formation of transverse dune fields. Earth Surf. Proc. Land. 25 (8), 905–918. https://doi.org/10.1002/1096-9837(200008)25:8<905::AID-ESP112>3.0.CO;2-Z.

Morelissen, R., Hulscher, S.J.M.H., Knaapen, M.A.F., Németh, A.A., Bijker, R., 2003. Mathematical modelling of sand wave migration and the interaction with pipelines. Coast. Eng. 48 (3), 197–209. https://doi.org/10.1016/S0378-3839(03)00028-0.

Nield, J.M., Baas, A.C.W., 2008. Investigating parabolic and nebkha dune formation using a cellular automaton modelling approach. Earth Surf. Proc. Land. 33 (5), 724–740. https://doi.org/10.1002/esp.1571.

Nishi, R., Sato, M., & Wang, H. (1995). Field observation and numerical simulation of beach and dune scarps *Coastal Engineering 1994* (pp. 2434-2448).

Nordstrom, K.F., McCluskey, J.M., 1984. Considerations for control of house construction in coastal dunes. Coastal Management 12 (4), 385–402. https://doi.org/10.1080/08920758409361972.

Nordstrom, K.F., McCluskey, J.M., 1985. The Effects of Houses and Sand Fences on the Eolian Sediment Budget at Fire Island, New York. J. Coastal Res. 1 (1), 39–46.

Oke, T.R., Mills, G., Christen, A., Voogt, J.A., 2017. Airflow *Urban Climates*. Cambridge University Press, Cambridge, pp. 77–121. https://doi.org/10.1017/9781139016476.005.

Peterka, J.A., Meroney, R.N., Kothari, K.M., 1985. Wind flow patterns about buildings. J. Wind Eng. Ind. Aerodyn. 21 (1), 21–38. https://doi.org/10.1016/0167-6105(85)90031-5.

Poppema, D. W., Wijnberg, K. M., Mulder, J. P. M., & Hulscher, S. J. M. H. (2022a). Experimental data of Deposition patterns around buildings at the beach: effects of building spacing and orientation: 4TU.ResearchData. doi:10.4121/16860145.v3.

Poppema, D.W., Wijnberg, K.M., Mulder, J.P.M., Vos, S., Hulscher, S.J.M.H., 2022b. Experimental data of The effect of building geometry on the size of aeolian deposition patterns: scale model experiments at the beach. 4TU.ResearchData. https://doi.org/10.4121/21285939.v2.

Poppema, D.W., Wijnberg, K.M., Mulder, J.P.M., Hulscher, S.J.M.H., 2019. Scale experiments on aeolian deposition and erosion patterns created by buildings on the beach. In: Wang, P., Rosatie, J.D., Vallee, M. (Eds.), Coastal Sediments 2019. World Scientific, pp. 1693–1707. https://doi.org/10.1142/9789811204487_0146.

Poppema, D.W., Wijnberg, K.M., Mulder, J.P.M., Vos, S.E., Hulscher, S.J.M.H., 2021. The effect of building geometry on the size of aeolian deposition patterns: scale model experiments at the beach. Coast. Eng. 103866 https://doi.org/10.1016/j.coastaleng.2021.103866.

Poppema, D.W., Wijnberg, K.M., Mulder, J.P.M., Hulscher, S.J.M.H., 2022c. Deposition patterns around buildings at the beach: effects of building spacing and orientation. Geomorphology. https://doi.org/10.1016/j.geomorph.2022.108114.

Pourteimouri, P., Campmans, G.H.P., Wijnberg, K.M., Hulscher, S.J.M.H., 2022. A Numerical Study on the Impact of Building Dimensions on Airflow Patterns and Bed Morphology around Buildings at the Beach. Journal of Marine Science and Engineering 10 (1), 13. https://doi.org/10.3390/jmse10010013.

Pye, K., Tsoar, H., 2008. Aeolian sand and sand dunes. Springer Science & Business Media. https://doi.org/10.1007/978-3-540-85910-9.

Qian, G., Dong, Z., Luo, W., Lu, J., 2011. Mean airflow patterns upwind of topographic obstacles and their implications for the formation of echo dunes: A wind tunnel simulation of the effects of windward slope. J. Geophys. Res. Earth Surf. 116 (F4) https://doi.org/10.1029/2011JF002020.

Reinders, J., Van der Valk, B., Van der Meulen, F., 2014. Effecten van tijdelijke strandbebouwing op de ontwikkeling van de jonge zeereep (H2130: Wit Duin) aan de zeezijde van de Duincompensie Delfstandse Kust (1206682–000-ZKS-0014). Deltares, Delft.

Roelvink, D., Costas, S., 2019. Coupling nearshore and aeolian processes: XBeach and duna process-based models. Environ. Modell. Software 115, 98–112. https://doi.org/10.1016/j.envsoft.2019.02.010.

Rotnicka, J., 2013. Aeolian vertical mass flux profiles above dry and moist sandy beach surfaces. Geomorphology 187, 27–37. https://doi.org/10.1016/j.geomorph.2012.12.032.

Sherman, D.J., Nordstrom, K.F., 1994. Hazards of Wind-Blown Sand and Coastal Sand Drifts: A Review. J. Coastal Res. 263–275.

Smith, A.B., Jackson, D.W.T., Cooper, J.A.G., 2017a. Three-dimensional airflow and sediment transport patterns over barchan dunes. Geomorphology 278, 28–42. https://doi.org/10.1016/j.geomorph.2016.10.025.

Smith, A.B., Jackson, D.W.T., Cooper, J.A.G., Hernández-Calvento, L., 2017b. Quantifying the role of urbanization on airflow perturbations and dunefield evolution. Earth's Future 5 (5), 520–539. https://doi.org/10.1002/2016ef000524.

Thiis, T.K., Jaedicke, C., 2000. The snowdrift pattern around two cubical obstacles with varying distance, measurements and numerical simulations. In: Hjorth-Hansen, E., Holand, I., Løset, S., Norem, H. (Eds.), Snow Engineering: Recent Advances and Developments. Trondheim, pp. 369–375. https://doi.org/10.1201/9780203739532.

Tsoar, H., 1983. Wind Tunnel Modeling of Echo and Climbing Dunes. In: Brookfield, M. E., Ahlbrandt, T.S. (Eds.), Developments in Sedimentology: Eolian Sediments and Processes, Vol. 38. Elsevier, pp. 247–259. https://doi.org/10.1016/S0070-4571(08)70798-2.

Tsoar, H., Blumberg, D., 1991. The effect of sea cliffs on inland encroachment of aeolian sand. In: Barndorff-Nielsen, O.E., Willetts, B.B. (Eds.), Aeolian Grain Transport, Vol. 2. Springer Vienna, Vienna, pp. 131–146. https://doi.org/10.1007/978-3-7091-6703-8_10.

Wang, W., Dun, H., He, W., Huang, N., 2020. Wind Tunnel Measurements of Surface Shear Stress on an Isolated Dune Downwind a Bridge. Applied Sciences 10 (11), 4022.

Werner, B.T., 1995. Eolian Dunes - Computer-Simulations and Attractor Interpretation. Geology 23 (12), 1107–1110. https://doi.org/10.1130/0091-7613(1995)023<1107:Edcsaa>2.3.Co;2.

Wilson, D.J., 1979. Flow patterns over flat roofed buildings and application to exhaust stack design. ASHRAE Trans. 85, 284–295.

Yan, N., Baas, A.C.W., 2017. Environmental controls, morphodynamic processes, and ecogeomorphic interactions of barchan to parabolic dune transformations. Geomorphology 278, 209–237. https://doi.org/10.1016/j.geomorph.2016.10.033.

Yen, S.C., Liu, C.T., 2011. Gap-flow patterns behind twin-cylinders at low Reynolds number. J. Mech. Sci. Technol. 25 (11), 2795–2803. https://doi.org/10.1007/s12206-011-0908-8.

Zhang, D., Narteau, C., Rozier, O., Courrech du Pont, S., 2012. Morphology and dynamics of star dunes from numerical modelling. Nat. Geosci. 5 (7), 463–467. https://doi.org/10.1038/ngeo1503.